CARBON 49 (2011) 3316–3324

available at www.sciencedirect.com

ScienceDirect

journal homepage: www.elsevier.com/locate/carbon

Diameter controlled growth of single-walled carbon nanotubes from SiO_2 nanoparticles

Yabin Chen, Jin Zhang *

Center for Nanochemistry, Beijing National Laboratory for Molecular Sciences, Key Laboratory for the Physics and Chemistry of Nanodevices, State Key Laboratory for Structural Chemistry of Unstable and Stable Species, College of Chemistry and Molecular Engineering, Peking University, Beijing 100871, PR China

ARTICLE INFO

Article history:
Received 26 January 2011
Accepted 7 April 2011
Available online 13 April 2011

ABSTRACT

A rational approach is reported for the growth of single-walled carbon nanotubes (SWCNTs) with controlled diameters using SiO_2 nanoparticles in a chemical vapor deposition system. The SiO_2 nanoparticles with different sizes were prepared by thermal oxidation of 3-aminopropyltriethoxysilane (APTES) with different number of layers which were assembled on Si substrates. It was found that the size of SiO_2 nanoparticles increased with the number of assembled APTES layers. Using these SiO_2 nanoparticles as nucleation centers, the diameter distribution of as-grown SWCNTs were correlated with the size of SiO_2 particles. In addition, both the classical longitudinal optical or transverse optical bands of SiC in *in situ* Raman spectra during the whole growth process and the Si 2p peak of SiC in the X-ray photoelectron spectra were not observed, suggesting that the carbon sources did not react with the SiO_2 nanoparticles during the growth. Comparing to vapor–liquid–solid mechanism for metallic catalysts, vapor–solid mechanism is proposed which results in a lower growth rate when using SiO_2 nanoparticles as nucleation centers.

1. Introduction

Single-walled carbon nanotubes (SWCNTs) have been regarded as one of the best candidates for future applications in many fields, such as nanoelectronics [1], thin-film materials [2], and sensor devices [3–5] due to their unique structures and superior electrical properties [6]. However, almost all currently available technologies for SWCNT growth, including arc discharge, laser ablation and catalytic chemical vapor deposition (CVD), can only produce mixtures of SWCNTs with a range of (*n*, *m*) indices [7], which is a large limitation for the application of SWCNTs. Therefore, how to grow SWCNTs with well-controlled structures is highly desirable for both fundamental research and practical applications.

Growth of SWCNTs with controlled structures and specifically with controlled chiralities is still in its infancy, although many papers have been published on this subject. Recently, much progress has been made towards growing SWCNTs with controlled diameters, conductive property or chirality [8]. Most of these works were based on the metallic catalytic CVD growth and the growth process complied with the classical vapor–liquid–solid (VLS) mechanism, which was similar to semiconducting nanowire growth [9]. In VLS growth process, the structure of SWCNT, especially the chirality of SWCNT is mostly determined by the initially formed cap structure around the surface of metal catalyst. However, it is difficult to control the cap structure by controlling the structure of metal catalysts at high temperature in CVD system [10]. It is more reasonable to reduce the diameter distribution of

* *Corresponding author:* Fax: +86 10 62757157.
E-mail address: jinzhang@pku.edu.cn (J. Zhang).
0008-6223/$ - see front matter
doi:10.1016/j.carbon.2011.04.016

SWCNTs than to control the chirality of SWCNTs by VLS mechanism. Meanwhile, it is a great challenge to completely remove the residual catalyst in metallic catalytic growth process, which could severely limit the application of SWCNTs in many fields [1,3,8].

In order to resolve problem of the residual metallic catalysts, some semiconductive nanoparticles, such as SiC, Si and Ge have been used to grow SWCNTs [11]. Moreover, these non-metallic nanoparticles also allowed for growth of SWCNTs with controlled structures. For example, the hexagonal silicon carbide could be used to grow SWCNTs with a narrow diameter distribution at the temperature above 1500 °C [12].

It is well known that the CVD system is a very complex process, and the diameter distribution of SWCNTs is influenced by many factors, such as growth temperature [13], gas flow rate [14], category of carbon source [15], type and size of the catalyst [16,17] and chamber pressure [18]. In metallic catalytic CVD growth process, the metal nanoparticles act as the nucleation centers for SWCNT growth [14] and thus there is a relationship between the catalyst size and SWCNT diameter. In our previous work, we found the diameters of SWCNTs grown from the single metallic nanoparticles could also be modulated by temperature [13]. Now there are also some works focused on trying to control SWCNT structure in terms of the nanoparticle topology. Some easily-removed mesoporous materials acted as templates to restrict the catalyst particle size [19–22]. In addition, the pre-treatment [23] and compositions of metal catalysts [16,24] were also investigated in order to modulate the SWCNT diameter. Depending on these methods SWCNTs with a narrow diameter distribution were produced [25,26], but it was still difficult to exactly control the SWCNT diameter, not to mention the desired (*n*, *m*) indices.

As mentioned above, the cap formed at the metal particle surface was stochastic due to inevitable thermal fluctuation during SWCNT growth. If so, we could attempt to control the structures of growing SWCNTs by taking advantage of the existed cap molecule or employing non-metal element with high melting point as the nucleation centers. In this way, the naturally deformed catalyst in liquid phase was avoided at the high growth temperature.

In our previous work, using the concept of SWCNT cloning, we developed a way to engineer the cap for SWCNT growth with controlled chirality. The open-end carbon structures, i.e., an existing SWCNT [27] or opened fullerene [28] were directly used as seeds to grow SWCNTs by open-end growth mode without introducing transition metal catalysts. Using the existing caps, the chirality of grown SWCNTs could be effectively controlled. However, the cloning growth efficiency was very low.

Last year, several groups sequentially reported that the deposited SiO_2 film [29] or scratched SiO_2 substrate can be successfully used to grow SWCNTs [30], which was a significant advancement in the field of SWCNT growth [31]. However, the growth velocity by metal-catalyst-free CVD processes was less than 10 nm/s, which was about 300 times slower than that with commonly used Co catalyst [32]. Due to their high melting point, it is generally assumed that the SiO_2 nanoparticles still remain in a solid state rather than melted state at the CNT growth temperature of 800–1000 °C. Furthermore, the cap structures and diameters of further formed SWCNTs can be easily controlled by using the special morphological SiO_2 nanoparticles as nucleation centers, meanwhile the adverse influences of residual metallic catalyst were excluded for the further application of SWCNTs. However the relationship between SiO_2 particle size and SWCNT diameter and the growth mechanism are still not resolved.

In the present study, we report a rational approach for the growth of SWCNTs with controlled diameters using SiO_2 nanoparticles of various sizes as nucleation centers. It was found that the SiO_2 nanoparticles ranged from 1.22 to 1.98 nm could be obtained by thermal oxidation of 3-aminopropyltriethoxysilane (APTES) with different number of assembled layers. Using these nanoparticles as nucleation centers, SWCNTs with diameters from 0.90 to 1.82 nm could be grown by ethanol-CVD, which indicated a direct relationship between SWCNT diameter and SiO_2 nanoparticle size. By *in situ* resonance Raman spectroscopy and X-ray photoelectron spectroscopy (XPS), we can prove that spherical SiO_2 nanoparticles did not transform into SiC while just played a role of nucleation centers during SWCNT growth. In this way, we suggest that the SWCNT growth process in our system follows vapor solid (VS) mechanism with a lower growth velocity. We believe that the obtained SWCNTs with controlled diameters by SiO_2 nanoparticles could facilitate their further application in more fields.

2. Experimental section

2.1. Self assembly of APTES layers

The APTES (⩾99%) was purchased from Acros Organics. The silicon wafer (boron doped, ⟨1 1 1⟩ plane) was cut into $1 \times 1\ cm^2$ slides as the substrates. These substrates were cleaned in Milli-Q water (>18.2 MΩ cm at pH 7.0), followed by ethanol, acetone and Milli-Q water again for 10 min, respectively. Then the Si substrates were immersed into piranha solution (7:3 sulfuric acid to hydrogen peroxide) at 90 °C for 30 min, then rinsed with Milli-Q water, and dried under nitrogen [33–35]. In order to prevent APTES from reacting with the glassware, the 10 ml glassware was prepared as described in [34]. APTES solution was diluted serially into the concentrations of 2×10^{-4}, 2×10^{-3}, 1.5×10^{-2} and 1.5×10^{-1} M in redistilled toluene, while operated in a glove box (H_2O and O_2 were <3 ppm). The prepared silicon substrates were immediately immersed into different APTES solutions at 25 °C for 30 min to assemble APTES layers. Finally the Si substrates were ultrasonically cleaned in redistilled chloroform for 5 min to remove the physisorbed APTES on the surface, and following rinsed with toluene, water and dried by a stream of nitrogen.

2.2. The fabrication of SiO_2 nanoparticles

The CVD system equipped with a new quartz boat and tube (1 in. interior diameter) was used [27]. Silicon substrates with different APTES layers were placed onto the quartz boat, and were oxidized at 900 °C for 15 min in air. In consequence, SiO_2 nanoparticles with different sizes were formed as the APTES

alkyl chains were removed [36]. More importantly, SiO_2 nanoparticles with larger diameter were formed when using APTES solutions with higher concentrations.

2.3. The growth of SWCNTs

SWCNTs were grown in CVD system equipped with new quartz boat and tube using ethanol vapor as carbon source. The substrates with SiO_2 nanoparticles were heated to 900 °C under a flow of Ar/H_2 (80/180 sccm) gas mixture, then the ethanol vapor by bubbling 80 sccm Ar was introduced into the furnace for SWCNT growth [29,30]. After 30 min growth, the ethanol vapor was turned off and the reactor was cooled to room temperature [27].

2.4. Characterization techniques

The surface functional groups and hydrophilicity of APTES layers were characterized by contact angle system (OCA30, Dataphysics Instruments GmbH, Germany). The thickness of APTES layers was confirmed by ellipsometer (Gaertner L 116B, angle of incidence was 70°, 633 nm laser). Atomic force microscopy (AFM, Nanoscope IIIA, operated at tapping mode) was used to verify the surface roughness of APTES layers and the diameters of oxidized SiO_2 nanoparticles and grown SWCNTs. Scanning electron microscopy (Hitachi S-4800, 1 kV) and Raman spectroscopy (Horiba HR800, 633 and 514 nm) showed the features and resonance modes of Si substrates and obtained SWCNTs. XPS (ESCALab250, Thermo Scientific Corporation) was used to confirm the chemical composition of the substrate surface.

3. Results and discussion

Fig. 1 presents a diagram of the preparation procedures from APTES layers to SiO_2 nanoparticles with controlled size, and followed by growth of SWCNTs in CVD. Firstly, different concentrations of APTES were prepared in redistilled toluene [33–35]. A series number of APTES layers were assembled onto the hydrophilic surface of silicon substrates in a glove box as shown in Fig. 1a. Secondly, the SiO_2 nanoparticles with different sizes were prepared by thermal oxidation of different number layers of assembled APTES in air. Finally, using the obtained SiO_2 nanoparticles as nucleation centers, SWCNTs with controlled diameter were grown on Si substrates using ethanol-CVD.

3.1. Characterization of self-assembled APTES layers

Fig. 2 displays the surface topographies of different numbers of APTES layers on silicon substrates. As shown in Fig. 2a, the thickness of APTES layers measured by ellipsometer, which indicated the larger concentrations of APTES solution was, the thicker APTES layers were assembled. As reported, the theoretical thickness of monolayer APTES was about 7 Å [35]. When assembling APTES layers with the concentrations of 2.0×10^{-3}, 1.5×10^{-2} and 1.5×10^{-1} M, the measured thicknesses were 3, 7 and 13 Å, which indicated assembled layers were sub-monolayer, monolayer and bilayer, respectively. Static contact angle was applicable to explain the surface properties, which was affected by many factors, such as conc entration, surface roughness and curing time. The measured contact angles in Fig. S1 illustrated the hydrophilic functional groups such as $–NH_2$ or –OH were predominant on the substrate surface [33,34]. Moreover, the surface of assembled layers became rougher with the number of APTES layer increasing. Typically as showed in Fig. 2d and e, root mean square roughness of monolayer and bilayer APTES were about 0.49 and 0.82 nm, respectively.

3.2. Characterization of SiO_2 nanoparticles

In order to obtain the SiO_2 nanoparticles, the APTES layers with different thicknesses were oxidized simultaneously at 900 °C for 15 min. During the oxidative process, the alkyl chains of APTES were firstly removed, and then the residual SiO_2 moved randomly on the silicon surface and aggregated into larger nanoparticles due to the less surface energies. Fig. 3a–d shows AFM images of SiO_2 nanoparticles obtained by oxidization of different APTES layers. We operated a statistical analysis about 70 SiO_2 nanoparticles to investigate the size distribution for each kind of APTES layers. The histograms in Fig. 3e–h show the size of SiO_2 nanoparticles became larger with increasing the APTES concentrations. That is because APTES layers with larger number were assembled, the more Si atoms on the substrates existed, and then the larger SiO_2 nanoparticles were formed. As the concentrations of APTES increasing from 2.0×10^{-4}, 2.0×10^{-3}, 1.5×10^{-2} to 1.5×10^{-1} M, the average diameters of SiO_2 nanoparticles increased from 1.22, 1.49, 1.67 to 1.98 nm. In general, the size scale of obtained nanoparticles is suitable to grow SWCNTs. Moreover, as shown in Fig. S2, only non-metallic elements, such as Si, O, C and N were observed in XPS spectra, which indicated there was no metallic contamination in our system.

3.3. Characterization of as-grown SWCNTs

With the SiO_2 nanoparticles of certain diameters, we suppose they could be utilized as the nucleation centers for SWCNT growth. As described in the Section 2, the silicon substrates with different size SiO_2 nanoparticles were placed in a 1 in. quartz tube with an Ar/H_2 (80/180 sccm) gas mixture. When temperature increased to 900 °C, ethanol vapor as carbon source was introduced into the furnace by bubbling 80 sccm Ar. After growth of 30 min, the system naturally cooled to room temperature [27,37].

SEM images in Fig. 4 show the un-oriented SWCNTs grown on Si substrates using SiO_2 nanoparticles with different sizes. The insets in Fig. 4a–d are AFM images of grown SWCNTs corresponding to APTES concentrations shown in Fig. 2b–e, respectively. Typical section analysis of AFM images of SWCNT is shown in Fig. S3. To explore the relationship between the size of SiO_2 nanoparticles and the diameter of SWCNTs, the diameter of about 70 SWCNTs for each APTES concentration were measured. Fig. 5a–d is the statistical histograms of the measured diameters of SWCNTs, which show that the diameters increased with the APTES concentration. When the sizes of SiO_2 nanoparticles were 1.22, 1.49, 1.67 and 1.98 nm in Fig. 3e–h, the diameters of SWCNTs were

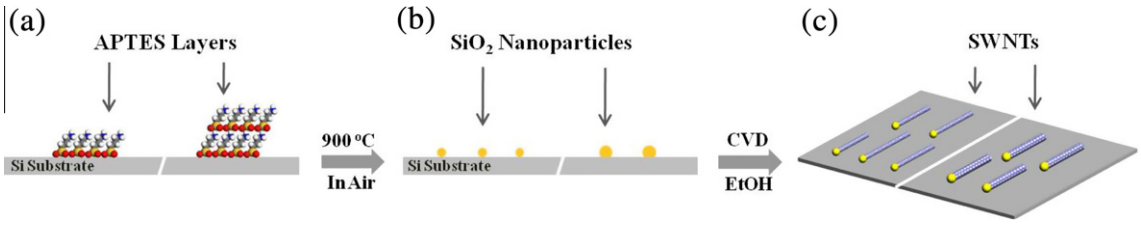

Fig. 1 – A diagram of diameter controlled growth of SWCNTs from SiO_2 nanoparticles. (a) APTES layers were assembled on the silicon substrates. (b) Discrete SiO_2 nanoparticles with desired size were obtained by thermal oxidization. (c) SWCNTs with controlled diameters were grown from obtained SiO_2 nanoparticles.

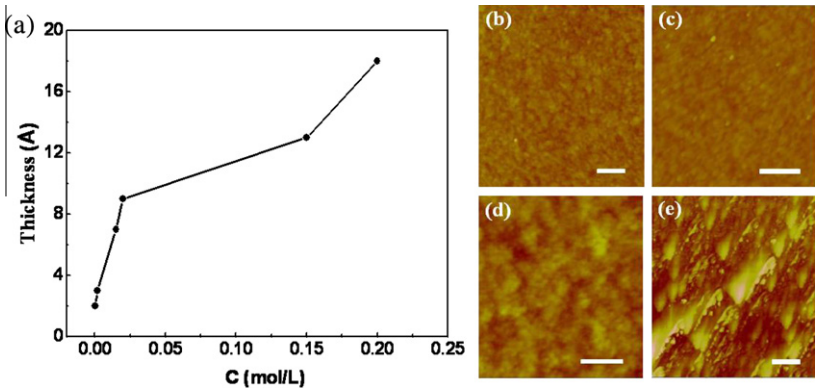

Fig. 2 – (a) Thickness variation of APTES layers as a function of solution concentrations. (b–e) AFM images of assembled APTES layers when the concentration was 2.0×10^{-4}, 2.0×10^{-3}, 1.5×10^{-2} and 1.5×10^{-1} M, respectively. The scale bars are 0.25 μm.

0.90, 1.26, 1.42 and 1.82 nm in Fig. 5a–d, respectively. For each APTES concentration, the diameter of grown SWCNTs was smaller than the size of oxidized SiO_2 nanoparticles, which was in accordance with relationships between the metallic nanoparticles and their grown SWCNTs [25]. The larger concentration of APTES solution was used, the larger diameter of SWCNTs was obtained. Furthermore, the Raman spectrum with RBM peak at 186.9 cm^{-1} of grown SWCNTs was shown in Fig. S3e, which corresponded to a SWCNT diameter of about 1.33 nm. Therefore, the diameter of SWCNTs can be simply and consistently controlled by adjusting the APTES concentrations.

3.4. *The growth mechanism of SWCNTs*

As shown in Fig. S4, we moved the SWCNT growth process in a mini-CVD system combined with *in situ* Raman spectroscopy. The mini-CVD is a closed heating stage (Linkam CCR1000) linked to all necessary gas sources. A quartz window was equipped on the top of sample chamber, which allowed the Raman laser to pass through the window without significant decay.

To exclude the resonance modes from Si substrate during the Raman characterization, 50 nm SiO_2 film was deposited onto Al_2O_3 substrates by electron beam evaporation. The Al_2O_3 substrate exhibited a sharp contrast in colors before (Fig. S5a) and after (Fig. S5b) deposition of SiO_2 films. The average size of SiO_2 particles was 2.07 nm as shown in Fig. S5c and d. The substrates were loaded into the mini-CVD chamber and then 180 sccm H_2 and ethanol vapor (80 sccm Ar bubbled through liquid ethanol) were introduced into the system. After focusing the 514 nm laser onto the SiO_2 surface for Raman measurement, the CVD chamber was heated to 900 °C at a rate of 100 °C/min. After reacting for 30 min, the system was cooled to room temperature. During the whole reaction process, Raman spectra were collected with a 10 s for every 50 °C. Typical Raman spectra were shown in Fig. 6a, including the spectra collected at the beginning of the growth (28–29 °C, black line), heating process (520–540 °C, red line[1]), growth process (900 °C, blue line), cooling (550–530 °C, cyan line) and after termination (33–32 °C, pink line). Raman signals from SiC were not observed, which should include the longitudinal optical band at 972 cm^{-1} and transverse optical band at 796 cm^{-1} [38,39]. Moreover, XPS spectra in Fig. 6b show that the peaks of Si 2p appear at 103.2 and 104.7 eV corresponding to SiO_x and $SiO_x(OH)_y$, respectively. In contrast, the Si 2p peak of SiC should appear at about 100.5 eV [40]. Obviously, both

[1] For interpretation to colour in the text, the reader is referred to the web version of this article.

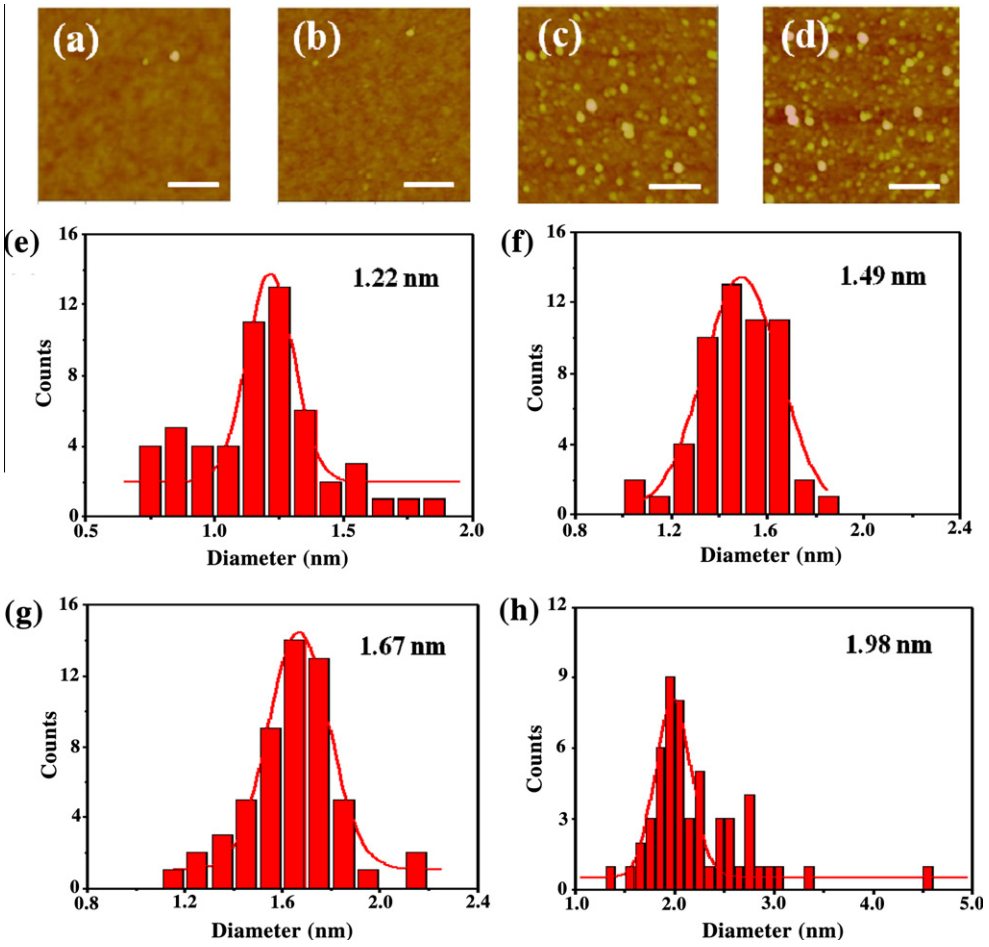

Fig. 3 – (a–d) AFM images of SiO_2 nanoparticles obtained by oxidization of the APTES layers which were prepared with the concentration of (a) 2.0×10^{-4}, (b) 2.0×10^{-3}, (c) 1.5×10^{-2}, and (d) 1.5×10^{-1} M. The scale bars are 0.25 μm. Corresponding histograms of nanoparticle size are plotted in (e–h), respectively. The red solid lines are Gaussian fitting peaks. (For interpretation of the references to colour in this figure legend, the reader is referred to the web version of this article.)

Raman spectroscopy and XPS revealed there was no SiC formed during the growth process. Therefore, the SiO_2 film did not react with carbon sources and remained its original chemical component. Moreover, the growth mechanism of SWCNTs from SiO_2 nanoparticles may be different from that by metallic nanoparticles.

In general, the SWCNT growth from metallic nanoparticles follows the VLS mechanism as shown in Fig. 7a [9]. Hydrocarbon fragments formed from decomposed carbon source (ethanol in this case) were transported with the gas stream, some of which randomly attacked the metallic nanoparticles and were chemically absorbed onto their surfaces. In accordance with metal–carbon phase diagram, carbon atoms on the particle surface would be dissolved into the nanoparticles and formed a solid-state solution at high temperature [41]. Once reaching the super-saturation point, the redundant carbon would precipitate into the SWCNT cap along the hemispherical surface [26,42]. Alternatively, a small fraction of carbon atoms could possibly bind with the edge of a SWCNT directly [43]. Some carbon atoms could also diffuse to the interfaces of SWCNT and nanoparticle along the surface, which would not form a solid-state solution in the bulk phase. Of course, all of these carbon atoms would contribute to SWCNT growth. Most kinds of metals, such as Fe, Co and Ni, have a great solubility to carbon, so the precipitated carbon is the major factor in SWCNT growth from metal catalyst [44]. In contrast, non-metallic elements like Si have little solubility to carbon according to their phase diagrams [45]. Raman spectroscopy and XPS characterization also indicated that no Si–C mixed phase formed and the SiO_2 nanoparticles retained their initial chemical components. Therefore, we speculate that the SWCNT grown from SiO_2 nanoparticle followed by a VS mechanism, which was different from metallic catalysts. Meanwhile, carbon atoms would experience a distinguished aggregation route to grow SWCNTs. As shown in Fig. 7b, the pyrolyzed carbon atoms can collide with SiO_2 nanoparticle and attach to its surface by unstable physisorption, and then diffused randomly along the SiO_2 surface. To reach a lower energy state, some carbon atoms bonded together into graphitized layers as the initial SWCNT cap. Otherwise, possibly a few carbon atoms would directly bond with the edge of the SWCNT. Because no Si–C alloy was formed, the SWCNT growth using SiO_2 nanoparticle is supposed to be followed a VS mechanism. Most recently, Cheng's group also proved that

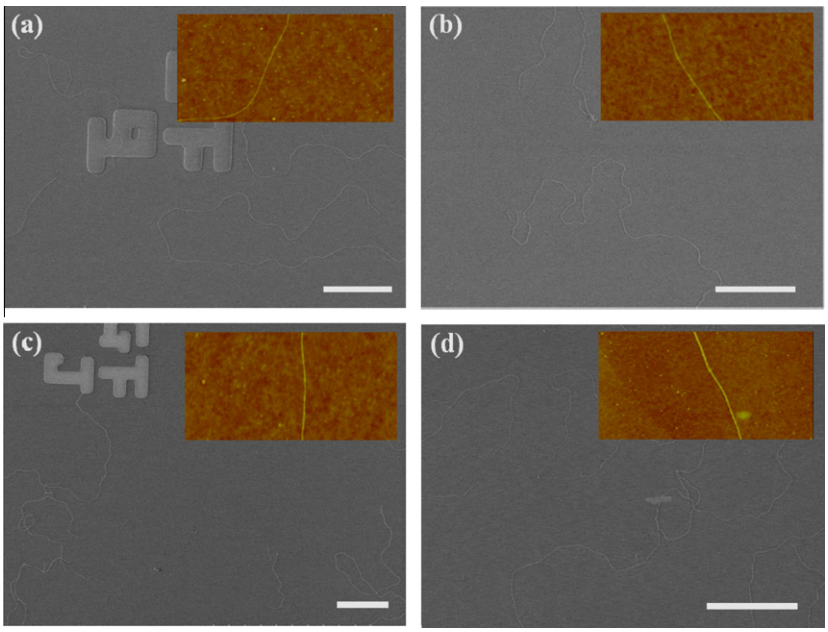

Fig. 4 – (a–d) SEM images of grown SWCNTs from different size SiO_2 nanoparticles corresponding to Fig. 3a–d. Insets are typical AFM images of SWCNTs. The scale bars are 15 μm.

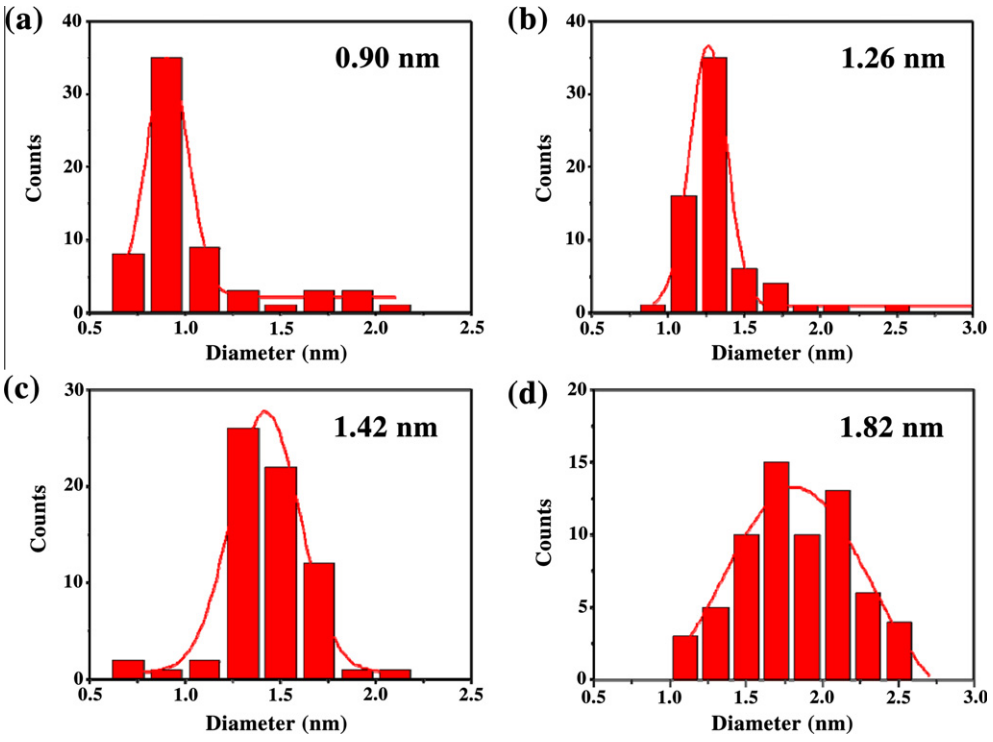

Fig. 5 – Histograms of SWCNT diameters grown from SiO_2 nanoparticles with size of 1.22 (a), 1.49 (b), 1.67 (c) and 1.98 nm (d), respectively. The red solid lines are Gaussian fitting peaks. (For interpretation of the references to colour in this figure legend, the reader is referred to the web version of this article.)

a vapor–solid–solid mechanism was suggested to the metal-free catalytic growth of SWCNTs from SiO_x [46], while Bachmatiuk's group was inclined to VLS mechanism when using quartz as both the silica support and provider of SiO_2 nanoparticles in spray CVD system [47]. So, the growth mechanism may depend on the growth conditions, which also needs more attentions.

As mentioned above, the mechanisms of SWCNT growth from metal or SiO_2 particles are different. From the principle of chemical dynamics, reaction rate was a function of the

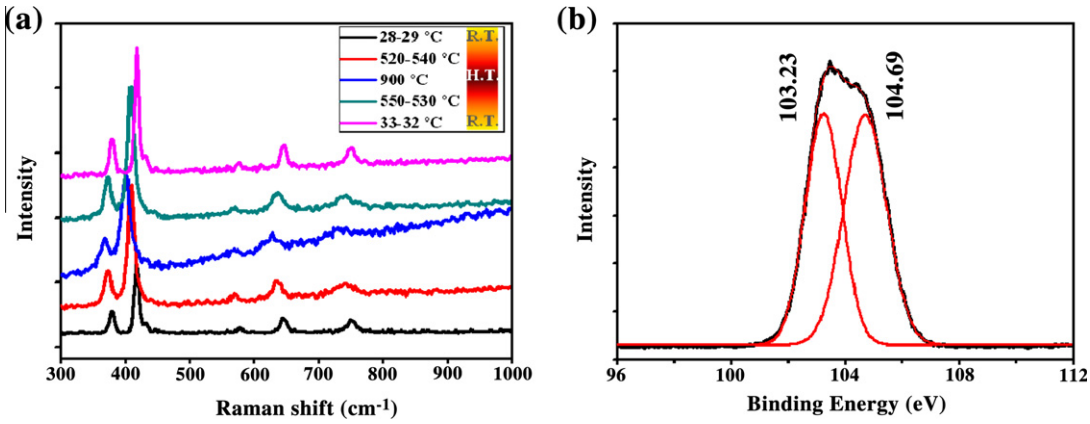

Fig. 6 – (a) *In situ* Raman spectra collected during the growth process in mini-CVD system. (b) XPS spectra of the SiO_2 film after SWCNT growth.

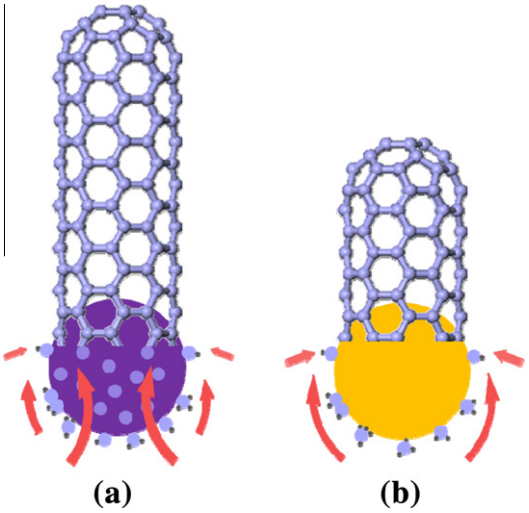

Fig. 7 – (a) The classical VLS mechanism during SWCNT growth by metallic catalyst. (b) The supposed VS mechanism during SWCNT growth from SiO_2 nanoparticles as nucleation centers.

concentration of reactants. VS mechanism should result in a slower growth rate than VLS mechanism, which was in agreement with experimental results [46]. In Fig. 4, SEM images illustrated that the length of obtained SWCNTs were around a few dozen micrometers, which was obviously shorter than samples by metal catalysts. SiO_2 nanoparticle only played a role of nucleation center for SWCNT growth. However, the metal cluster as a chemical catalyst could further promote the decomposition of carbon source, which resulted in a superior efficiency and faster growth rate than that with SiO_2 nanoparticles. At this point, the exact way by which carbon atoms were transported onto the SiO_2 particle surface and the mechanism by which carbon atoms could gather into a SWCNT cap were still interesting issues towards understanding chirality-selective growth of SWCNTs.

4. Conclusions

In conclusion, a rational method is put forward to control the diameter of SWCNTs in an ethanol-CVD system without metallic nanoparticles. The size of SiO_2 nanoparticles obtained by thermal oxidation increased with concentration of APTES solutions. Using these nanoparticles as nucleation centers, the diameters of grown SWCNTs, ranged from 0.90 to 1.82 nm, were related to the size of SiO_2 nanoparticles. Furthermore, VS mechanism was supposed to interpret the growth process of SWCNTs. Although the SWCNT growth rate was relatively slower than that from metal nanoparticles, we believe that the obtained SWCNTs, totally free of residual metal, would have a further application in nanoelectronics.

Acknowledgments

This work was supported by NSFC (50972001, 20725307 and 50821061) and MOST (2011CB932601, 2007CB936203).

Appendix A. Supplementary data

Supplementary data associated with this article can be found, in the online version, at doi:10.1016/j.carbon.2011.04.016.

REFERENCES

[1] Tans SJ, Verschueren ARM. Room-temperature transistor based on a single carbon nanotube. Nature 1998;393(6680):49–52.
[2] Hu LB, CHoi JW, Yang Y, Jeongb S, Mantiaa FL, Cui LF, et al. Highly conductive paper for energy-storage devices. Proc Natl Acad Sci USA 2009;106(51):21490–4.
[3] Yang WR, Ratinac KR, Ringer SP, Thordarson P, Gooding JJ, Braet F. Carbon nanomaterials in biosensors: should you use nanotubes or graphene? Angew Chem Int Ed 2010;49(12):2114–38.

[4] Li J, Liu YJ, Ye Q, Cinke M, Han J, Meyyappan M. Carbon nanotube sensors for gas and organic vapor detection. Nano Lett 2003;3(7):929–33.
[5] Modi A, Koratkar N, Lass E, Wei BQ, Ajayan PM. Miniaturized gas ionization sensors using carbon nanotubes. Nature 2003;424(6945):171–4.
[6] Iijima S, Ichiashi T. Single-shell carbon nanotubes of 1-nm diameter. Nature 1993;363(6430):603–5.
[7] Kumar M, Ando Y. Chemical vapor deposition of carbon nanotubes: a review on growth mechanism and mass production. J Nanosci Nanotechnol 2010;10(6):3739–58.
[8] Liu ZF, Jiao LY, Yao YG, Xian XJ, Zhang J. Aligned, ultralong single-walled carbon nanotubes: from synthesis, sorting, to electronic devices. Adv Mater 2010;22(21):2285–310.
[9] Hu JT, Odom T, Lieber CM. Chemistry and physics in one dimension: synthesis and properties of nanowires and nanotubes. Acc Chem Res 1999;32(5):435–45.
[10] Zhu WM, Börjesson A, Bolton K. DFT and tight binding Monte Carlo calculations related to single-walled carbon nanotube nucleation and growth. Carbon 2010;48(2):470–8.
[11] Takagi D, Hibino H, Suzuki S, Kobayashi Y, Homma Y. Carbon nanotube growth from semiconductor nanoparticles. Nano Lett 2007;7(8):2272–5.
[12] Derycke V, Martel R, Radosavljevic M, Ross FM, Avouris P. Catalyst-free growth of ordered single-walled carbon nanotube networks. Nano Lett 2002;2(10):1043–6.
[13] Yao YG, Li QW, Zhang J, Liu R, Jiao LY, Zhu YTT, et al. Temperature-mediated growth of single-walled carbon nanotube intramolecular junctions. Nat Mater 2007;6(4):283–6.
[14] Kuo CS, Bai A, Huang CM, Li YY, Hu CC, Chen CC. Diameter control of multiwalled carbon nanotubes using experimental strategies. Carbon 2005;43(13):2760–8.
[15] Maruyama S, Miyauchi Y, Edamura T, Igarashi Y, Chiashi S, Murakami Y. Synthesis of single-walled carbon nanotubes with narrow diameter-distribution from fullerene. Chem Phys Lett 2003;375(5–6):553–9.
[16] Chiang WH, Sankaran PM. Linking catalyst composition to chirality distributions of as-grown single-walled carbon nanotubes by tuning Ni_xFe_{1-x} nanoparticles. Nat Mater 2009;8(11):882–6.
[17] Lolli G, Zhang L, Balzano L, Sakulchaicharoen N, Tan YQ, Resasco DE. Tailoring (*n*, *m*) structure of single-walled carbon nanotubes by modifying reaction conditions and the nature of the support of CoMo catalysts. J Phys Chem B 2006;110(5):2108–15.
[18] Hiraoka T, Bandow S, Shinohara H, Iijima S. Control on the diameter of single-walled carbon nanotubes by changing the pressure in floating catalyst CVD. Carbon 2006;44(9): 1845–69.
[19] Schmidt I, Boisen A, Gustavsson E, Ståhl K, Pehrson S, Dahl S, et al. Carbon nanotube templated growth of mesoporous zeolite single crystals. Chem Mater 2001;13(12):4416–8.
[20] Liu X, Bigioni TP, Xu Y, Cassell AM, Cruden BA. Vertically aligned dense carbon nanotube growth with diameter control by block copolymer micelle catalyst templates. J Phys Chem B 2006;110(41):20102–6.
[21] Li CY, Zhu HW, Suenaga K, Wei JQ, Wang KL, Wu DH. Diameter dependent growth mode of carbon nanotubes on nanoporous SiO_2 substrates. Mater Lett 2009;63(15):1366–9.
[22] Duesberg GS, Graham AP, Liebau M, Seidel R, Unger E, Kreupl F, et al. Growth of isolated carbon nanotubes with lithographically defined diameter and location. Nano Lett 2003;3(2):257–9.
[23] Nessim GD, Hart AJ, Kim JS, Acquaviva D, Oh J, Morgan CD, et al. Tuning of vertically-aligned carbon nanotube diameter and areal density through catalyst pre-treatment. Nano Lett 2008;8(11):3587–93.
[24] Li N, Wang XM, Derrouiche S, Haller GL, Pfefferle LD. Role of surface cobalt silicate in single-walled carbon nanotube synthesis from silica-supported cobalt catalysts. Acs Nano 2010;4(3):1759–67.
[25] Cheung CL, Kurtz A, Park H, Lieber CM. Diameter-controlled synthesis of carbon nanotubes. J Phys Chem B 2002;106(10):2429–33.
[26] Li YM, Kim W, Zhang YG, Rolandi M, Wang DW, Dai HJ. Growth of single-walled carbon nanotubes from discrete catalytic nanoparticles of various sizes. J Phys Chem B 2001;105(46):11424–31.
[27] Yao YG, Feng CQ, Zhang J, Liu ZF. "Cloning" of single-walled carbon nanotubes via open-end growth mechanism. Nano Lett 2009;9(4):1673–7.
[28] Yu XC, Zhang J, Choi WM, Choi YJ, Kim JM, Gan LB, et al. Cap formation engineering: from opened C_{60} to single-walled carbon nanotubes. Nano Lett 2010;10(9):3343–9.
[29] Liu BL, Ren WC, Gao LB, Li SS, Pei SF, Liu C, et al. Metal-catalyst-free growth of single-walled carbon nanotubes. J Am Chem Soc 2009;131(6):2082–3.
[30] Huang SM, Cai QR, Chen YJ, Qian Y, Zhang LJ. Metal-catalyst-free growth of single-walled carbon nanotubes on substrates. J Am Chem Soc 2009;131(6):2094–5.
[31] Liu HP, Takagi D, Chiashi S, Homma Y. The growth of single-walled carbon nanotubes on a silica substrate without using a metal catalyst. Carbon 2010;48(1):114–22.
[32] Liu BL, Ren WC, Liu C, Sun CH, Gao LB, Li SS, et al. Growth velocity and direct length-sorted growth of short single-walled carbon nanotubes by ametal-catalyst-free chemical vapor deposition process. Acs Nano 2009;3(11):3421–30.
[33] Howarter JA, Youngblood JP. Optimization of silica silanization by 3-aminopropyltriethoxysilane. Langmuir 2006;22(26):11142–7.
[34] Vandenberg ET, Bertilsson L, Liedberg B, Uvdal K, Erlandsson R, Elwing H, et al. Structure of 3-aminopropyl triethoxy silane on silicon oxide. J Colloid Interface Sci 1991;147(1):103–18.
[35] Chauhan AK, Aswal DK, Koiry SP, Gupta SK, Yakhmi JV, Surgers C, et al. Self-assembly of the 3-aminopropyltrimethoxysilane multilayers on Si and hysteretic current–voltage characteristics. Appl Phys A 2008;90(3):581–9.
[36] Horii NM, Okimura K, Shibata A. Investigation of SiO_2 deposition processes with mass spectrometry and optical emission spectroscopy in plasma enhanced chemical vapor deposition using tetraethoxysilane. Thin Solid Films 1999;343–344:148–51.
[37] Hong G, Zhang B, Peng BH, Zhang J, Choi WM, Choi JY, et al. Direct growth of semiconducting single-walled carbon nanotube array. J Am Chem Soc 2009;131(41):14642–3.
[38] Bechelany M, Brioude A, Cornu D, Ferro G, Miele P. A Raman spectroscopy study of individual SiC nanowires. Adv Funct Mater 2007;17(6):939–43.
[39] Chollon G. Structural and textural analyses of SiC-based and carbon CVD coatings by Raman microspectroscopy. Thin Solid Films 2007;516(2–4):388–96.
[40] Emtsev KV, Bostwick A, Karsten H, Jobst J, Kellogg GL, Ley L, et al. Towards wafer-size graphene layers by atmospheric pressure graphitization of silicon carbide. Nat Mater 2009;8(3):203–7.
[41] Schaper AK, Hou HQ, Greiner A, Phillipp F. The role of iron carbide in multiwalled carbon nanotube growth. J Catal 2004;222(1):250–4.
[42] Kong J, Soh HT, Cassell AM, Quate CF, Dai HJ. Synthesis of individual single-walled carbon nanotubes on patterned silicon wafers. Nature 1998;395(6705):878–81.

[43] Hofmann S, Csanyi G, Ferrari AC, Payne MC, Robertson J. Surface diffusion: the low activation energy path for nanotube growth. Phys Rev Lett 2005;95(3):36101–4.
[44] Fan X, Buczko R, Puretzky AA, Geohegan DB, Howe JY, Pantelides ST, et al. Nucleation of single-walled carbon nanotubes. Phys Rev Lett 2003;90(14):145501–4.
[45] Abbaschian GJ, Olesinski RW. The C–Si (carbon–silicon) system. Bull Alloy Phase Diagrams 1984;5(5):486–9.
[46] Liu BL, Tang DM, Sun CH, Liu C, Ren WC, Li F, et al. Importance of oxygen in the metal-free catalytic growth of single-walled carbon nanotubes from SiO_x by a vapor–solid–solid mechanism. J Am Chem Soc 2011;133(2):197–9.
[47] Bachmatiuk A, Börrnert F, Grobosch M, Schäffel F, Wolff U, Scott A, et al. Investigating the graphitization mechanism of SiO_2 nanoparticles in chemical vapor deposition. Acs Nnao 2009;3(12):4098–104.